

This supplementary information was **updated** on **08/11/2021**.

### **Rashba exciton in a 2D perovskite quantum dot**

The authors regret that the production code used for plots in the electronic supplementary information contained an error in the calculation of oscillator strengths. As such, the production code has been updated in the accompanying .zip folder, and Figures S3 and S4 have been updated as displayed herein. The previous versions of these Figures and captions are displayed immediately below for future reference of the reader. A summary of the changes to the Figures is as follows:

- Fig S3: Colors of some points in the  $F_z=1$  plots (middle row in the figure) were previously incorrect and subsequently updated.
- Fig S4: Oscillator strength line plots in panels (d) and (h) were incorrect and subsequently updated. Caption has been modified as panel (d) in the figure is qualitatively different when corrected.

Please contact [Nanoscale@rsc.org](mailto:Nanoscale@rsc.org) with any inquiries, citing the DOI: [doi.org/10.1039/D1NR04884H](https://doi.org/10.1039/D1NR04884H)

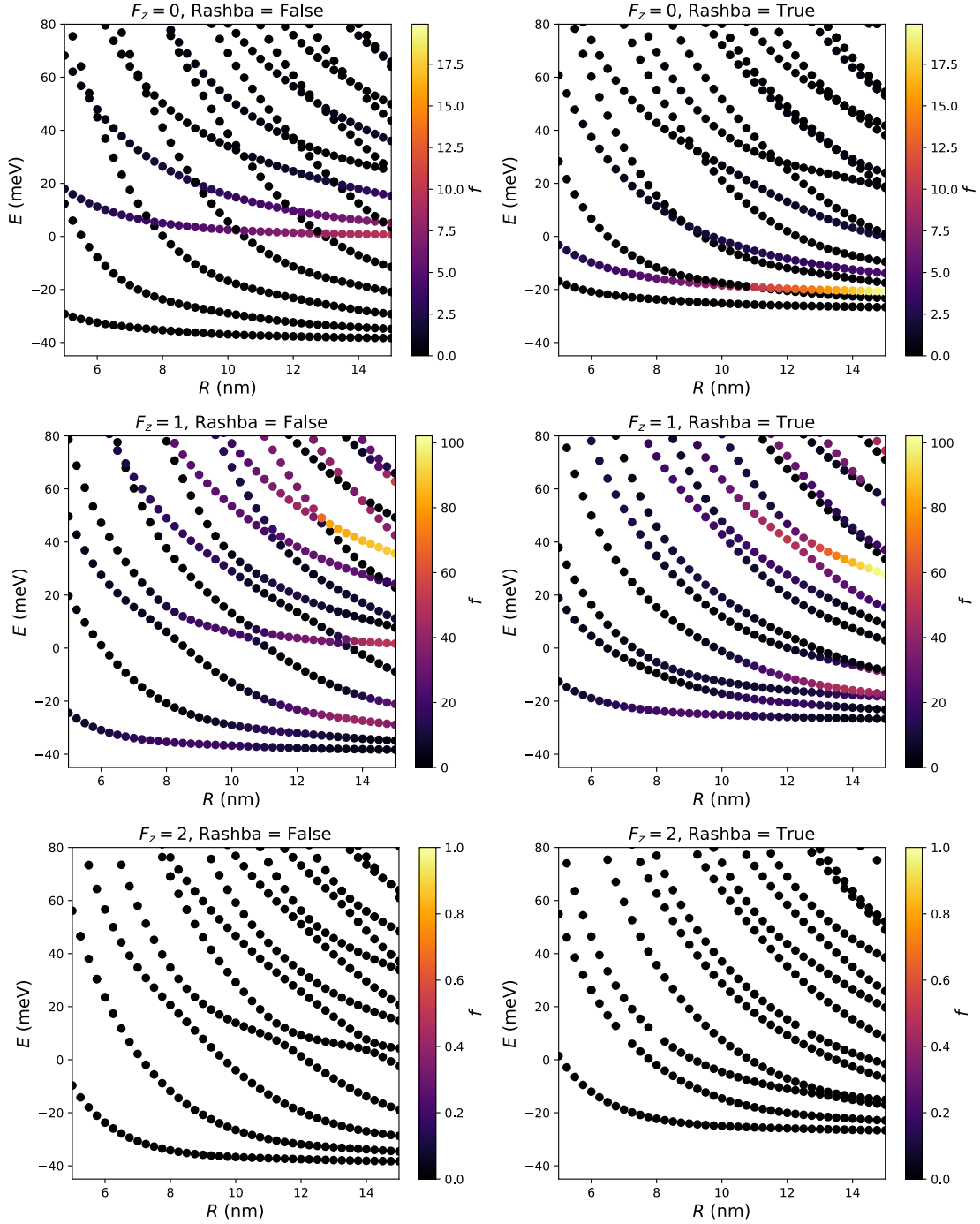


Figure S-3. Energy levels of confined wavefunctions as a function of disk radius  $R$  (as in Figure 3) but without the LR exchange corrections. Rows are  $F_z = 0$  (top),  $F_z = 1$  (middle), and  $F_z = 2$  (bottom), and columns are without and with internal Rashba from the left. The total oscillator strength  $f$  of the states as given by Eq. (26) is indicated by the color of the points. The results are qualitatively very similar to Figure 3. The avoided crossings can be seen more easily in this version, since the LR contribution is not included self-consistently in the wavefunctions.

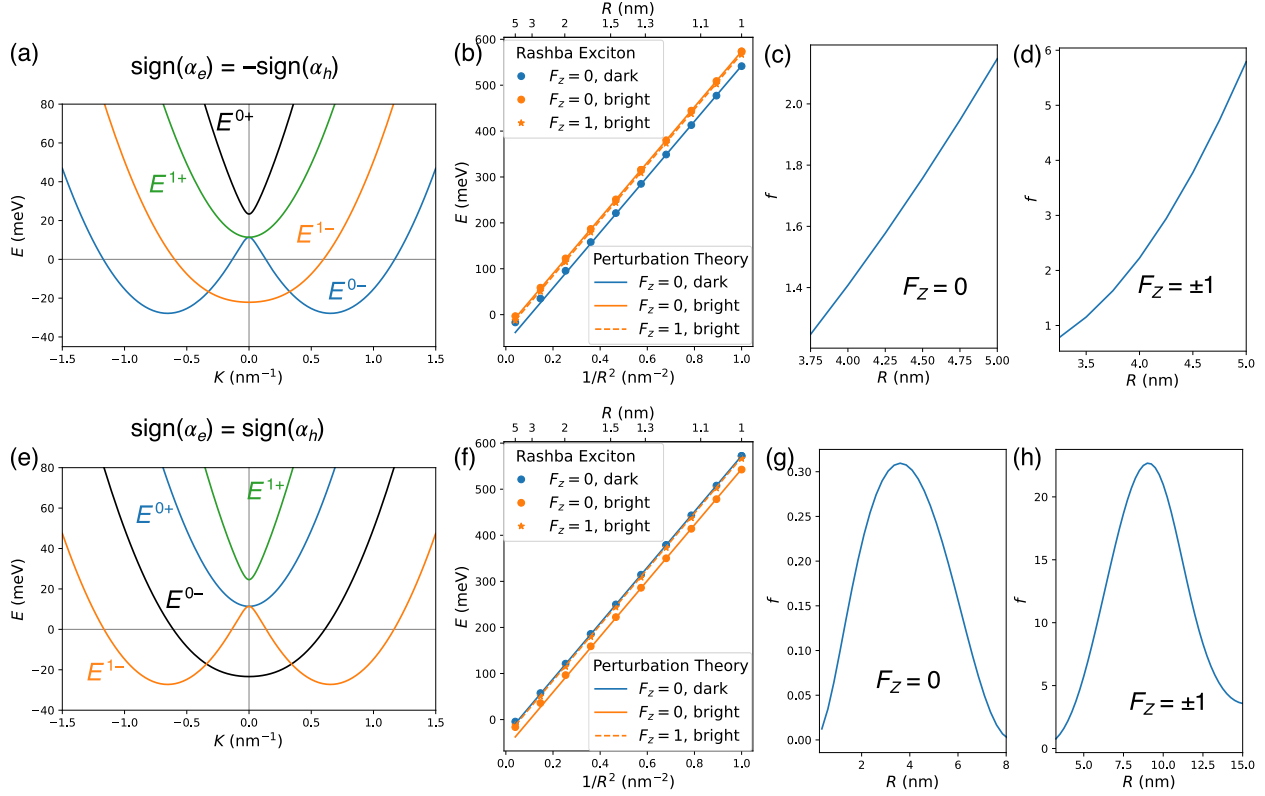


Figure S-4. Comparison of same-sign and opposite-sign cases for small QDs. Panels (a-d) use the opposite sign for  $\alpha_e$  and  $\alpha_h$  (as is assumed elsewhere in the paper) while panels (e-h) use the same sign. (a) and (e) show the dispersion. (b) and (f) show the energy levels (neglecting LR exchange) for small QDs as a function of  $1/R^2$ . As expected, we see four parallel lines (dark and bright  $F_z = 0$ , two degenerate  $F_z = \pm 1$ ) with the dark and bright  $F_z = 0$  states switching position between the cases. The energies approach the results from perturbation theory, which are shown by lines and described by  $E^{F_z}(R) = \frac{\hbar^2(2.405)^2}{2MR^2} - 2A_r^{\text{COM}}(E_r^e + E_r^h) + E_{\text{exch}}^{F_z}$ , where the first term represents COM confinement, the second term is an overall shift due to COM Rashba terms in Eq. 2, and the exchange terms  $E_{\text{exch}}^{F_z}$  represent the sum of SR exchange and Rashba internal motion terms. The exchange terms are given by  $E_{\text{exch}}^{F_z=1} = w \cos^2 \theta$ ,  $E_{\text{exch}}^{F_z=0, \text{bright}} = 2w \sin^2 \theta - 4(A_r^{\text{COM}} - A_r^{\text{REL}})\mathcal{E}_R$ , and  $E_{\text{exch}}^{F_z=0, \text{dark}} = 4(A_r^{\text{COM}} - A_r^{\text{REL}})\mathcal{E}_R$ .  $A_r^{\text{COM}} \approx 0.48$  is the COM Rashba coefficient [9] and  $A_r^{\text{REL}} \approx 0.292$  is the relative Rashba coefficient. Oscillator strengths (OS) are shown as a function of  $R$  in panels (c, d, g, h). In the opposite-sign case, OS of the  $F_z = 0$  bright state (c) and  $F_z = \pm 1$  bright state (d) are monotonically increasing with  $R$ . In the same-sign case, the OS of the  $F_z = 0$  bright state (g) and  $F_z = \pm 1$  bright state (h) show peaks at intermediate  $R$  and go to zero in both the  $R \rightarrow 0$  limit (as expected from the perturbative treatment [9]) and the  $R \rightarrow \infty$  limit (due to the indirect nature of the bulk dispersion).

**Electronic Supplementary Information:**  
**Rashba exciton in a 2D perovskite quantum dot**

Michael W. Swift<sup>a,1</sup> John L. Lyons,<sup>1</sup> Alexander L. Efros,<sup>1</sup> and Peter C. Sercel<sup>2,3</sup>

<sup>1</sup>*Center for Computational Materials Science,*

*U.S. Naval Research Laboratory, Washington D.C. 20375, United States*

<sup>2</sup>*Department of Applied Physics and Materials Science,*

*California Institute of Technology, Pasadena, California 91125, United States*

<sup>3</sup>*Center for Hybrid Organic Inorganic Semiconductors for Energy,*

*Golden, Colorado 80401, United States*

**CONTENTS**

List of Figures	1
I. Rashba exciton dispersion	2
II. Separation of variables	3
III. Branch decoupling	6
IV. Negative or complex $K^2$	11
V. Oscillator transition strength	13
VI. Long-range exchange	16
References	21

**LIST OF FIGURES**

S-1 Variational Results .....	17
S-2 Long-range exchange corrections .....	18

---

<sup>a</sup> ASEE Postdoctoral Fellow

S-3	Levels without long-range exchange .....	19
S-4	Small QDs in the perturbative regime .....	20
S-5	Bright ground exciton .....	21

## I. RASHBA EXCITON DISPERSION

The transformation from the electron-hole pair basis from Refs. 1–3 to the angular momentum basis  $|J, J_z\rangle$  basis we used for the effective Rashba exchange,  $\tilde{Q} = \langle P|J, J_z\rangle$ , can be written by direct inspection:

$$\tilde{Q} = \begin{pmatrix} 0 & 1 & 0 & 0 \\ -\frac{1}{\sqrt{2}} & 0 & \frac{1}{\sqrt{2}} & 0 \\ \frac{1}{\sqrt{2}} & 0 & \frac{1}{\sqrt{2}} & 0 \\ 0 & 0 & 0 & 1 \end{pmatrix}. \quad (\text{S1})$$

The eigenvectors of Eq. (15) given in Eq. (17) involve  $c$  coefficients which are given by:

$$c_{\pm 1}(K) = -\frac{(E_t - E_z) \mp \sqrt{4(\alpha_{\text{ex}}^+)^2 K^2 + (E_t - E_z)^2}}{2\alpha_{\text{ex}}^+ K} \quad (\text{S2})$$

$$c_{0\pm}(K) = \frac{(E_t - E_d) \mp \sqrt{4(\alpha_{\text{ex}}^-)^2 K^2 + (E_d - E_t)^2}}{2\alpha_{\text{ex}}^- K}. \quad (\text{S3})$$

The four independent momenta  $K_{1\pm}$  and  $K_{0\pm}$  found by solving Eq. (16) for a given exciton energy  $E$  are:

$$\begin{aligned} \hbar^2 K_{1\pm}^2 &= 2M \left( E - \mathcal{E}_{0,0} - \frac{E_t + E_z}{2} \right) + 2 \left( \frac{M\alpha_{\text{ex}}^+}{\hbar} \right)^2 \\ &\pm \sqrt{4 \left( \frac{M\alpha_{\text{ex}}^+}{\hbar} \right)^4 + 8M \left( \frac{M\alpha_{\text{ex}}^+}{\hbar} \right)^2 \left( E - \mathcal{E}_{0,0} - \frac{E_t + E_z}{2} \right) + M^2 (E_t - E_z)^2} \\ \hbar^2 K_{0\pm}^2 &= 2M \left( E - \mathcal{E}_{0,0} - \frac{E_d + E_t}{2} \right) + 2 \left( \frac{M\alpha_{\text{ex}}^-}{\hbar} \right)^2 \\ &\pm \sqrt{4 \left( \frac{M\alpha_{\text{ex}}^-}{\hbar} \right)^4 + 8M \left( \frac{M\alpha_{\text{ex}}^-}{\hbar} \right)^2 \left( E - \mathcal{E}_{0,0} - \frac{E_d + E_t}{2} \right) + M^2 (E_d - E_t)^2}. \end{aligned} \quad (\text{S4})$$

As discussed in the main text, the exciton has its minimum energy  $\mathcal{E}_{\text{min}}$  on a circle in  $K$ -space defined by  $K_x^2 + K_y^2 = K_{\text{R}}^2$ , where

$$\mathcal{E}_{\text{min}} = \mathcal{E}_{0,0} + \frac{E_d + E_t}{2} - \frac{M(\alpha_{\text{ex}}^-)^2}{2\hbar^2} - \frac{(E_d - E_t)^2 \hbar^2}{8M(\alpha_{\text{ex}}^-)^2}, \quad K_{\text{R}}^2 = \frac{(M\alpha_{\text{ex}}^-)^2}{\hbar^4} - \frac{(E_d - E_t)^2}{4(\alpha_{\text{ex}}^-)^2}. \quad (\text{S5})$$

Low-energy excitons near this minimum experience no dispersion in the polar direction and parabolic dispersion in the radial direction:

$$\mathcal{E}_{\min}(\mathbf{K}) = \mathcal{E}_{\min} + \frac{\hbar^2(|\mathbf{K}| - K_{\text{R}})^2}{2M_{\min}} . \quad (\text{S6})$$

The local effective mass at the minimum  $M_{\min}$  is given by

$$M_{\min} = M \frac{4M^2(\alpha_{\text{ex}}^-)^4}{4M^2(\alpha_{\text{ex}}^-)^4 - (E_{\text{d}} - E_{\text{t}})^2\hbar^4} . \quad (\text{S7})$$

The density of exciton states,  $D(E)$ , near this minimum has one-dimensional character. Indeed

$$D(E) = \frac{A}{(2\pi)^2} \int dK_x dK_y \delta(E - \mathcal{E}_{\min}(\mathbf{K})) , \quad (\text{S8})$$

where  $A$  is the 2D surface area. Using the cylindrical symmetry of the minimum we arrive at the density of exciton states per unit area

$$\frac{D(E)}{A} = \frac{K_{\text{R}}}{2\pi\hbar} \frac{\sqrt{2M_{\min}}}{\sqrt{E - \mathcal{E}_{\min}}} . \quad (\text{S9})$$

The coefficients  $c_{1,1}$ ,  $c_{1,2}$ ,  $c_{0,1}$ , and  $c_{0,2}$  used in Section 3 are defined based on Eq. (S3) analogously to Eq. (21):

$$\begin{aligned} c_{1,1} &= \begin{cases} c_{1+} & \text{if } E^{1+}(K_{1+}) = E \\ c_{1-} & \text{if } E^{1-}(K_{1+}) = E \end{cases} \\ c_{1,2} &= \begin{cases} c_{1+} & \text{if } E^{1+}(K_{1-}) = E \\ c_{1-} & \text{if } E^{1-}(K_{1-}) = E \end{cases} \\ c_{0,1} &= \begin{cases} c_{0+} & \text{if } E^{0+}(K_{0+}) = E \\ c_{0-} & \text{if } E^{0-}(K_{0+}) = E \end{cases} \\ c_{0,2} &= \begin{cases} c_{0+} & \text{if } E^{0+}(K_{0-}) = E \\ c_{0-} & \text{if } E^{0-}(K_{0-}) = E . \end{cases} \end{aligned} \quad (\text{S10})$$

Derived material parameters for the model are given in Supplementary Table S-1.

## II. SEPARATION OF VARIABLES

In this section we explicitly carry out the separation of variables in a quantum disk. Substituting the wavefunction from Eq. (14) into Eq. (13) where all momenta are considered

Parameter	Value (no internal Rashba)	Value (including internal Rashba, if different)
$A_{\text{R}}^{\mathcal{L}}$	0	0.292
$a_{1,0}$	2.805 nm	
$E_{1,0}$	-415.2 meV	
$a_{2,1}$	1.385 nm	
$E_{2,1}$	-122.9 meV	
$m_e$	0.182 $m_0$	
$m_h$	0.182 $m_0$	
$\mathcal{E}_{\text{R}}$	0	-20 meV
$\alpha_e$	183 meV nm	
$\alpha_h$	-91.5 meV nm	
$E_{\text{d}}$	0 meV	23.4 meV
$E_{\text{t}}$	1.2 meV	
$E_z$	11.4 meV	-12.0 meV
$E_{\text{min}}$	-44.4 meV	-33.4 meV
$a_x$	3.55 nm	
$g_0$	0.321	
$g_1$	0.974	
$\tilde{\epsilon}_{\infty}$	3.5	
$\hbar\omega_{\text{LT}}$	20.8 meV	

Table S-1. Derived PEPI parameters, assuming  $m_e = m_h$ ,  $\alpha_e > 0$ , and  $\alpha_h < 0$ . Where applicable, values are shown both without and with internal Rashba.

as momenta operator and presenting operators  $\hat{K}_{\pm}$  and  $\hat{\mathbf{K}}^2$  in cylindrical coordinates;

$$\hat{\mathbf{K}}^2 = - \left[ \frac{1}{\rho} \frac{\partial}{\partial \rho} \rho \frac{\partial}{\partial \rho} + \frac{1}{\rho^2} \frac{\partial^2}{\partial \phi^2} \right], \quad \hat{K}_{\pm} = -ie^{\pm i\phi} \left[ \frac{\partial}{\partial \rho} \pm \frac{i}{\rho} \frac{\partial}{\partial \phi} \right]. \quad (\text{S11})$$

We obtain the equations describing the radial component of the wavefunction  $\mathcal{R}$

$$\begin{aligned}
& \left[ \mathcal{E}_{0,0} - E - \frac{\hbar^2}{2M} \Delta_{F_z} \right] \mathcal{R}_{0,0}^{F_z} + \frac{\alpha_{\text{ex}}^-}{\sqrt{2}} A_{F_z-1}^+ \mathcal{R}_{1,+1}^{F_z} - \frac{\alpha_{\text{ex}}^-}{\sqrt{2}} A_{F_z+1}^- \mathcal{R}_{1,-1}^{F_z} = 0, \\
& \frac{\alpha_{\text{ex}}^-}{\sqrt{2}} A_{F_z}^- \mathcal{R}_{0,0}^{F_z} - \left[ \mathcal{E}_{0,0} + \Delta - E - \frac{\hbar^2}{2M} \Delta_{F_z-1} \right] \mathcal{R}_{1,1}^{F_z} + \frac{\alpha_{\text{ex}}^+}{\sqrt{2}} A_{F_z}^- \mathcal{R}_{1,0} = 0, \\
& \frac{\alpha_{\text{ex}}^+}{\sqrt{2}} A_{F_z-1}^+ \mathcal{R}_{1,+1}^{F_z} - \left[ \mathcal{E}_{0,0} + \Delta + \delta - E - \frac{\hbar^2}{2M} \Delta_{F_z} \right] \mathcal{R}_{1,0}^{F_z} + \frac{\alpha_{\text{ex}}^+}{\sqrt{2}} A_{F_z+1}^- \mathcal{R}_{1,-1}^{F_z} = 0, \\
& -\frac{\alpha_{\text{ex}}^-}{\sqrt{2}} A_{F_z}^+ \mathcal{R}_{0,0}^{F_z} + \frac{\alpha_{\text{ex}}^+}{\sqrt{2}} A_{F_z}^+ \mathcal{R}_{1,0}^{F_z} - \left[ \mathcal{E}_{0,0} + \Delta - E - \frac{\hbar^2}{2M} \Delta_{F_z+1} \right] \mathcal{R}_{1,-1}^{F_z} = 0, \quad (\text{S12})
\end{aligned}$$

where the radial operators  $\Delta_\ell$  and  $A_\ell^\pm$  are defined as:

$$\Delta_\ell = \frac{1}{\rho} \frac{\partial}{\partial \rho} \rho \frac{\partial}{\partial \rho} - \frac{\ell^2}{\rho^2}, \quad A_\ell^- = \left[ \frac{\partial}{\partial \rho} + \frac{\ell}{\rho} \right], \quad A_\ell^+ = - \left[ \frac{\partial}{\partial \rho} - \frac{\ell}{\rho} \right]. \quad (\text{S13})$$

For free exciton motion, the equations for the radial function are satisfied by Bessel functions with integer index,  $J_\ell(K\rho)$ , where  $\ell = 0, 1, 2, \dots$ . Using the relationship  $\Delta_\ell J_\ell(K\rho) = -K^2 J_\ell(K\rho)$  and  $A_\ell^\pm J_\ell(K\rho) = K I_{\ell\pm 1}(K\rho)$ , we can reduce the problem of the variable separation to the solution of a  $4 \times 4$  matrix. Indeed substituting  $\mathcal{R}_{0,0}^{F_z}(\rho) = C_{0,0}^{F_z} J_{F_z}(K\rho)$  and  $\mathcal{R}_{1,\nu}^{F_z}(\rho) = C_{1,\nu}^{F_z} J_{F_z-\nu}(K\rho)$ , where  $\nu = \pm 1, 0$ . We obtain the Hamiltonian given in Eq. (15),

$$\hat{H}_{F_z} = \begin{pmatrix} |0,0\rangle|F_z\rangle & |1,1\rangle|F_z-1\rangle & |1,0\rangle|F_z\rangle & |1,-1\rangle|F_z+1\rangle \\ \mathcal{E}_{0,0} + \frac{\hbar^2 K^2}{2M} & \frac{1}{\sqrt{2}} K \alpha_{\text{ex}}^- & 0 & -\frac{1}{\sqrt{2}} K \alpha_{\text{ex}}^- \\ \frac{1}{\sqrt{2}} K \alpha_{\text{ex}}^- & \mathcal{E}_{0,0} + E_t + \frac{\hbar^2 K^2}{2M} & \frac{1}{\sqrt{2}} K \alpha_{\text{ex}}^+ & 0 \\ 0 & \frac{1}{\sqrt{2}} K \alpha_{\text{ex}}^+ & \mathcal{E}_{0,0} + E_z + \frac{\hbar^2 K^2}{2M} & \frac{1}{\sqrt{2}} K \alpha_{\text{ex}}^+ \\ -K \alpha_{\text{ex}}^- & 0 & \frac{1}{\sqrt{2}} K \alpha_{\text{ex}}^+ & \mathcal{E}_{0,0} + E_t + \frac{\hbar^2 K^2}{2M} \end{pmatrix}. \quad (\text{S14})$$

To diagonalize the Hamiltonian we transform it according to:

$$\hat{\mathcal{H}}'_{F_z} = \tilde{m}^{-1} \hat{H}_{F_z} \tilde{m}, \quad \tilde{m} = \begin{pmatrix} 1 & 0 & 0 & 0 \\ 0 & \frac{-1}{\sqrt{2}} & \frac{1}{\sqrt{2}} & 0 \\ 0 & 0 & 0 & 1 \\ 0 & \frac{1}{\sqrt{2}} & \frac{1}{\sqrt{2}} & 0 \end{pmatrix}, \quad (\text{S15})$$

resulting in the basis  $|0,0\rangle|F_z\rangle$ ,  $|B_1\rangle$ ,  $|B_2\rangle$ ,  $|1,0\rangle|F_z\rangle$  with

$$|B_1\rangle = \frac{-1}{\sqrt{2}} [|1,1\rangle|F_z-1\rangle - |1,-1\rangle|F_z+1\rangle], \quad (\text{S16})$$

$$|B_2\rangle = \frac{1}{\sqrt{2}} [|1,1\rangle|F_z-1\rangle + |1,-1\rangle|F_z+1\rangle]. \quad (\text{S17})$$

. The Hamiltonian in this basis is block diagonal:

$$\hat{\mathcal{H}}'_{F_z} = \begin{pmatrix} |0,0\rangle|F_z\rangle & |B_1\rangle & |B_2\rangle & |1,0\rangle|F_z\rangle \\ \mathcal{E}_{0,0} + \frac{\hbar^2 K^2}{2M} & -K\alpha_{\text{ex}}^- & 0 & 0 \\ -K\alpha_{\text{ex}}^- & \mathcal{E}_{0,0} + E_t + \frac{\hbar^2 K^2}{2M} & 0 & 0 \\ 0 & 0 & \mathcal{E}_{0,0} + E_t + \frac{\hbar^2 K^2}{2M} & K\alpha_{\text{ex}}^+ \\ 0 & 0 & K\alpha_{\text{ex}}^+ & \mathcal{E}_{0,0} + E_z + \frac{\hbar^2 K^2}{2M} \end{pmatrix}. \quad (\text{S18})$$

The block-diagonal form allows analytic diagonalization, resulting in Eq. 16:

$$E_{F_z}^{1\pm}(K) = \mathcal{E}_{0,0} + \frac{\hbar^2 K^2}{2M} + \frac{E_t + E_z}{2} \pm \frac{\sqrt{(E_t - E_z)^2 + 4K^2(\alpha_{\text{ex}}^+)^2}}{2},$$

$$E_{F_z}^{0\pm}(K) = \mathcal{E}_{0,0} + \frac{\hbar^2 K^2}{2M} + \frac{E_d + E_t}{2} \pm \frac{\sqrt{(E_d - E_t)^2 + 4K^2(\alpha_{\text{ex}}^-)^2}}{2}.$$

with eigenvectors given by

$$|\mathbf{E}_{F_z}^{1\pm}\rangle = c_{1\pm}|B_2\rangle + |1,0\rangle|F_z\rangle, \quad |\mathbf{E}_{F_z}^{0\pm}\rangle = c_{0\pm}|0,0\rangle|F_z\rangle + |B_1\rangle, \quad (\text{S19})$$

By substituting in Eq. (S16) and Eq. (S17), and using Eq. (S3) we can write the eigenvectors as column vectors in the product basis of Eq. (S14), arriving at Eq. (17):

$$|\mathbf{E}_{F_z}^{1\pm}\rangle = \frac{1}{\sqrt{1 + c_{1\pm}^2(K)}} \begin{pmatrix} 0 \\ c_{1\pm}(K)/\sqrt{2} \\ 1 \\ c_{1\pm}(K)/\sqrt{2} \end{pmatrix}, \quad |\mathbf{E}_{F_z}^{0\pm}\rangle = \frac{1}{\sqrt{1 + c_{0\pm}^2(K)}} \begin{pmatrix} c_{0\pm}(K) \\ -1/\sqrt{2} \\ 0 \\ 1/\sqrt{2} \end{pmatrix}.$$

### III. BRANCH DECOUPLING

#### A. Special case $F_z = 0$

##### 1. Decoupling for the $E^{0\pm}$ exciton branches

Let us examine the basis vectors Eq. (S16) that comprise part of the solution of the  $E^{0\pm}$  energy branch for  $F_z = 0$ . The envelope coordinate representation of basis vector  $|B_1\rangle$  is,

$$\langle\rho, \phi|B_1\rangle = \frac{-1}{\sqrt{2}} (|1,1\rangle\langle\rho, \phi|F_z - 1\rangle - |1,-1\rangle\langle\rho, \phi|F_z + 1\rangle), \quad (\text{S20})$$

$$\langle\rho, \phi|B_1\rangle = \frac{-1}{\sqrt{2}} e^{iF_z\phi} (|1,1\rangle e^{-i\phi} J_{F_z-1}(K\rho) - |1,-1\rangle e^{i\phi} J_{F_z+1}(K\rho)). \quad (\text{S21})$$

Let us consider the very simple special case  $F_z = 0$ . Then,

$$\langle \rho, \phi | B_1(F_z = 0) \rangle = \frac{-1}{\sqrt{2}} (|1, 1\rangle e^{-i\phi} J_{-1}(K\rho) - |1, -1\rangle e^{i\phi} J_1(K\rho)) . \quad (\text{S22})$$

Now let us use the identity  $J_{-1}(x) = J_1(x)$ . Then,

$$\langle \rho, \phi | B_1(F_z = 0) \rangle = \frac{1}{\sqrt{2}} (|1, 1\rangle e^{-i\phi} + |1, -1\rangle e^{i\phi}) J_1(K\rho) . \quad (\text{S23})$$

This shows that for  $F_z = 0$  the ket  $|B_1\rangle$  has associated with it only a *single* radial function.

The same argument can be applied to the  $|B_2\rangle$  ket.

Putting this in vector form we can write, for the special case of  $F_z = 0$ , the radial coordinate representation of the energy eigenvectors for the  $E^{0\pm}$  branch:

$$\begin{aligned} \langle \rho, \phi | \mathbf{E}_{F_z=0}^{0\pm}(K) \rangle &= \frac{1}{\sqrt{1 + c_{0\pm}^2(K)}} \begin{pmatrix} c_{0\pm}(K) J_0(K\rho) \\ -1/\sqrt{2} e^{-i\phi} J_{-1}(K\rho) \\ 0 \\ 1/\sqrt{2} e^{i\phi} J_1(K\rho) \end{pmatrix} \\ &= \frac{1}{\sqrt{1 + c_{0\pm}^2(K)}} \begin{pmatrix} c_{0\pm}(K) J_0(K\rho) \\ 1/\sqrt{2} e^{-i\phi} J_1(K\rho) \\ 0 \\ 1/\sqrt{2} e^{i\phi} J_1(K\rho) \end{pmatrix} . \end{aligned} \quad (\text{S24})$$

Since within the  $E^{0\pm}$  branch there are two solutions for  $K$  for a given energy, which we label  $K_1$  and  $K_2$ , the total wavefunction for  $F_z = 0$ , for the  $E^{0\pm}$  branch can be written as the sum of the 0 branch bulk eigenvectors with roots  $K_1$  and  $K_2$ , which may correspond to the  $E^{0-}$ ,  $E^{0+}$ , or both branches at a given energy:

$$\Psi_{F_z=0}^{0\pm}(\rho) = A \langle \rho, \phi | \mathbf{E}_{F_z=0}^{0\pm}(K_1) \rangle + B \langle \rho, \phi | \mathbf{E}_{F_z=0}^{0\pm}(K_2) \rangle , \quad (\text{S25})$$

which can satisfy the boundary condition for a disk of radius  $R$ ,

$$\Psi_{F_z=0}^0(\rho = R) = 0 , \quad (\text{S26})$$

because the solution involves two radial equations with two unknowns ( $A, B$ ). Since within Eq. (S24) there are only two independent rows, the value of the energy that causes the first and the fourth rows to vanish will also cause the second row to vanish. Therefore the  $F_z = 0$  state associated with branch  $E^{0\pm}$  completely decouples from the branch  $E^{1\pm}$ .

2. *Decoupling for the  $E^{1\pm}$  exciton branches.*

Examining Eq. (17): we can also see that the same arguments made above for the  $E^{0\pm}$  exciton branches can be used to write decoupled solutions for the  $E^{1\pm}$  branch. We rewrite the coordinate representation of the  $E^{1\pm}$  energy eigenvectors for  $F_z = 0$  as,

$$\langle \rho, \phi | \mathbf{E}_{F_z=0}^{1\pm}(K) \rangle = \frac{1}{\sqrt{1 + c_{\pm 1}^2(K)}} \begin{pmatrix} 0 \\ c_{\pm 1}(K)/\sqrt{2}e^{-i\phi}(-J_1(K\rho)) \\ J_0(K\rho) \\ c_{\pm 1}(K)/\sqrt{2}e^{i\phi}J_1(K\rho) \end{pmatrix}. \quad (\text{S27})$$

We note that the radial wavefunction in the second element in this vector is proportional to the fourth. Proceeding on, since there are two independent solutions for  $K$  in branch 1 at a given energy, which we label  $K_3$ ,  $K_4$ , we can form now the quantum disk wavefunction as a combination of the two corresponding energy eigenvectors:

$$\Psi_{F_z=0}^1(\rho) = C \langle \rho, \phi | \mathbf{E}_{F_z=0}^{1\pm}(K_3) \rangle + D \langle \rho, \phi | \mathbf{E}_{F_z=0}^{1\pm}(K_4) \rangle. \quad (\text{S28})$$

This wavefunction can satisfy the boundary condition,

$$\Psi_{F_z=0}^1(\rho = R) = 0, \quad (\text{S29})$$

because a solution involves two equations in the two unknowns,  $C, D$ . Since within Eq. (S29) there are only two independent rows, the quantum confined state associated with branch 1 completely decouples from the branch 0 for  $F_z = 0$ .

**B. General case  $F_z \neq 0$**

Now let us consider if the decoupling of the  $E^{0\pm}$  and  $E^{1\pm}$  exciton branches is possible in the general case  $F_z \neq 0$ . We examine the energy eigenvectors for this branch. Let us examine the radial coordinate representation of the energy eigenvectors for the  $E^{0\pm}$  branch:

$$\langle \rho, \phi | \mathbf{E}^{0\pm}(K) \rangle = \frac{e^{iF_z\phi}}{\sqrt{1 + c_{0\pm}^2(K)}} \begin{pmatrix} c_{0\pm}(K)J_{F_z}(K\rho) \\ -1/\sqrt{2}e^{-i\phi}J_{F_z-1}(K\rho) \\ 0 \\ 1/\sqrt{2}e^{i\phi}J_{F_z+1}(K\rho) \end{pmatrix}. \quad (\text{S30})$$

This wavefunction has cylindrical symmetry and can be written for two distinct values of  $K$ , however, each of the 3 components of this wavefunction should vanish at the QD surface. Let us check if this is possible. We will try the decoupling procedure using the following identity,

$$J_{n-1}(x) + J_{n+1}(x) = \frac{2n}{x} J_n(x), \quad (\text{S31})$$

or better

$$J_n(x) = (x/2n)[J_{n-1}(x) + J_{n+1}(x)], \quad (\text{S32})$$

which allows us to rewrite the energy eigenvectors for the  $E^{0\pm}$  branch as,

$$\langle \rho, \phi | \mathbf{E}^{0\pm}(K) \rangle = \frac{e^{iF_z\phi}}{\sqrt{1 + c_{0\pm}^2(K)}} \begin{pmatrix} c_{0\pm}(K)(K\rho/2F_z)[J_{F_z-1}(K\rho) + J_{F_z+1}(K\rho)] \\ -1/\sqrt{2}e^{-i\phi} J_{F_z+1}(K\rho) \\ 0 \\ 1/\sqrt{2}e^{i\phi} J_{F_z+1}(K\rho) \end{pmatrix}. \quad (\text{S33})$$

The corresponding eigenvectors for the  $E^{1\pm}$  branch are,

$$\langle \rho, \phi | \mathbf{E}^{1\pm}(K) \rangle = \frac{e^{iF_z\phi} c_{1\pm}(K)}{\sqrt{1 + c_{1\pm}^2(K)}} \begin{pmatrix} 0 \\ 1/\sqrt{2}e^{-i\phi} J_{F_z-1}(K\rho) \\ 1/c_{1\pm}(K)(K\rho/2F_z)[J_{F_z-1}(K\rho) + J_{F_z+1}(K\rho)] \\ 1/\sqrt{2}e^{i\phi} J_{F_z+1}(K\rho) \end{pmatrix}. \quad (\text{S34})$$

It appears that the radial wavefunction in the first and third rows in these expressions is a linear combination of the ones in the second and fourth rows.

Let us consider now if the boundary condition requirement that the radial wave function vanish at the surface in each row can be satisfied in this case with just two  $K$ :  $K_1$  and  $K_2$ . Consider again our general quantum disk superposition of two bulk vectors, Eq. (S25), which was written for the case  $F_z = 0$ . Let us suppose that such a wavefunction can be written for the general case,  $F_z \neq 0$ . In that event, we suppose a wave function of the form,

$$\Psi_{F_z}^{0\pm}(\rho) = A \langle \rho, \phi | \mathbf{E}_{F_z}^{0\pm}(K_1) \rangle + B \langle \rho, \phi | \mathbf{E}_{F_z}^{0\pm}(K_2) \rangle.$$

In this case our wavefunction is a mix of branch 0 states with wave vectors  $K_1$  and  $K_2$  respectively:

$$\Psi_{F_z}^{0\pm}(\rho) = A \begin{pmatrix} c_{0\pm}(K_1) \frac{K_1\rho}{2F_z} [J_{F_z-1}(K_1\rho) + J_{F_z+1}(K_1\rho)] \\ -1/\sqrt{2}e^{-i\phi} J_{F_z+1}(K_1\rho) \\ 0 \\ 1/\sqrt{2}e^{i\phi} J_{F_z+1}(K_1\rho) \end{pmatrix} + B \begin{pmatrix} c_{0\pm}(K_2) \frac{K_2\rho}{2F_z} [J_{F_z-1}(K_2\rho) + J_{F_z+1}(K_2\rho)] \\ -1/\sqrt{2}e^{-i\phi} J_{F_z+1}(K_2\rho) \\ 0 \\ 1/\sqrt{2}e^{i\phi} J_{F_z+1}(K_2\rho) \end{pmatrix}.$$

Now consider the boundary condition at radius  $R$ :  $\Psi_{F_z=0}^{0\pm}(\rho = R) = 0$ . Writing out all components of the vector equation explicitly,

$$\begin{aligned} Ac_0(K_1)J_{F_z}(K_1R) + Bc_0(K_2)J_{F_z}(K_2R) &= 0 , \\ AJ_{F_z-1}(K_1R) + BJ_{F_z-1}(K_2R) &= 0 , \\ AJ_{F_z+1}(K_1R) + BJ_{F_z+1}(K_2R) &= 0 . \end{aligned} \quad (\text{S35})$$

Now we add the second and third of these equations together and use identity Eq. (S31):  $J_{n-1}(x) + J_{n+1}(x) = \frac{2n}{x}J_n(x)$ , we obtain,

$$A\frac{J_{F_z}(K_1R)}{K_1} + B\frac{J_{F_z}(K_2R)}{K_2} = 0 . \quad (\text{S36})$$

Now our system of equations reduces to,

$$\begin{aligned} Ac_0(K_1)J_{F_z}(K_1R) + Bc_0(K_2)J_{F_z}(K_2R) &= 0 , \\ A\frac{J_{F_z}(K_1R)}{K_1} + B\frac{J_{F_z}(K_2R)}{K_2} &= 0 . \end{aligned} \quad (\text{S37})$$

One can see that we are apparently able to satisfy BCs and find the energy of confined levels in the branch 0 solutions:

$$[(c_0(K_1)/K_2) - (c_0(K_2)/K_1)]J_{F_z}(K_1a)J_{F_z}(K_2a) = 0 . \quad (\text{S38})$$

Equation Eq. (S38) indicates that there are two solutions: (1)  $A = 0$  and  $J_{F_z}(K_2R) = 0$  and (2)  $B = 0$   $J_{F_z}(K_1R) = 0$ . However, neither solution causes all three rows in Eq. (S35) to vanish at the surface. We conclude that there is no decoupling for  $|F_z| > 0$ . For  $F_z = 0$ , decoupling occurs due to the fact that  $J_1(x) = J_{-1}(x)$ .

The same argument can be made for the existence of decoupled branch 1 solutions.

$$\Psi_{F_z}^1(\rho) = C\langle\rho, \phi|\mathbf{E}_{F_z=0}^{1\pm}(K_3)\rangle + D\langle\rho, \phi|\mathbf{E}_{F_z=0}^{1\pm}(K_4)\rangle .$$

In this case our wavefunction has the form of a mix of branch 1 states with wave vectors  $K_3$  and  $K_4$  respectively:

$$\Psi_{F_z}^1(\rho) = C \begin{pmatrix} 0 \\ 1/\sqrt{2}e^{-i\phi}J_{F_z-1}(K_3\rho) \\ \frac{1}{c_{1\pm}(K_3)}\frac{K_3\rho}{2F_z}[J_{F_z-1}(K_3\rho) + J_{F_z+1}(K_3\rho)] \\ 1/\sqrt{2}e^{i\phi}J_{F_z+1}(K_3\rho) \end{pmatrix} + D \begin{pmatrix} 0 \\ 1/\sqrt{2}e^{-i\phi}J_{F_z-1}(K_4\rho) \\ \frac{1}{c_{1\pm}(K_4)}\frac{K_4\rho}{2F_z}[J_{F_z-1}(K_4\rho) + J_{F_z+1}(K_4\rho)] \\ 1/\sqrt{2}e^{i\phi}J_{F_z+1}(K_4\rho) \end{pmatrix} .$$

Similar considerations as outlined above for the 0-branch shows that decoupling is impossible for the 1-branch for  $|F_z| > 0$ .

Consequently the quantum confined state associated with  $F_z \neq 0$  must be an admixture between the  $E^{0\pm}$  and the  $E^{1\pm}$  branches. This can be seen in the numerical results, which show avoided crossings for  $F_z \neq 0$  but not for  $F_z = 0$  (Figure 3).

#### IV. NEGATIVE OR COMPLEX $K^2$

In this section, we prove that the boundary conditions are sufficient and the wavefunctions can be chosen to be real, despite the occurrence of complex  $K^2$  values. We first consider the case where some  $K^2$  are negative but all are real. In this case, some  $K$  are pure imaginary, and the corresponding  $c$  coefficients in the wave function are also imaginary. An integer Bessel function of an imaginary argument is either pure real or pure imaginary:  $J_\ell(ix) \propto i^\ell$ . The corresponding eigenvectors (19),(20) are thus either pure real or pure imaginary, depending on the parity of  $F_z$ :  $E^{0\pm}$  is real for even  $F_z$  and imaginary for odd  $F_z$ , while  $E^{1\pm}$  is real for odd  $F_z$  and imaginary for even  $F_z$ . The determinant in Eq (24) is real with an even number of imaginary rows or imaginary with an odd number. In a coupled system ( $F_z \neq 0$ ), all  $A, B, C, D$  coefficients are real or imaginary in order to give the correct sign of the determinant, so the overall wavefunction is purely real or purely imaginary. In a decoupled system, the same argument applies within the decoupled 2x2 block.

We now consider complex  $K^2$ . If  $E$  is below the minimum of the dispersion, all four  $K$  are complex and the situation is unphysical. However, in the case  $E_{\min} < E < \mathcal{E}_{0,0} + \frac{E_t + E_z}{2}$ ,  $K_{1+}^2$  and  $K_{1-}^2$  are complex, and both correspond to the  $E^{1-}$  branch. At this energy, both  $K_{0\pm}$  are real. The coefficients  $A, B$  cannot vanish in general (this would represent a decoupled solution, which does not exist for  $F_z \neq 0$  as proved in Supplementary Section III) so they must be complex. One might be concerned that this leads to additional degrees of freedom requiring additional boundary conditions. However, we will show that this is not the case.

We begin by noting that  $K_{1\pm}^2$  are complex when the argument of the square root in Eq. (S4) is negative, so  $K_{1+}^* = K_{1-}$ . (Note  $\sqrt{z}$  is the principle square root of  $z$  in all cases). Since both  $K_{1+}$  and  $K_{1-}$  are from the  $E_{1-}$  branch, it can be shown that

$c_{1,1} = c_{1-}(K_{1+}) = c_{1-}(K_{1-}^*) = (c_{1-}(K_{1-}))^* = c_{1,2}^*$ . Therefore the first two columns of the matrix in Eq. (24) are complex conjugates of one another. Let  $\mathbf{v}_1$  be the real part of the first column,  $\mathbf{v}_2$  be its imaginary part, and  $\mathbf{v}_3$  and  $\mathbf{v}_4$  be the third and fourth columns. We consider cases.

### Case 1

First, assume  $\mathbf{v}_3$  and  $\mathbf{v}_4$  are both real. This happens when  $K_{0\pm}^2$  is positive and in some cases where it is negative (as discussed above). Eq. (24) may then be rewritten

$$A(\mathbf{v}_1 + i\mathbf{v}_2) + B(\mathbf{v}_1 - i\mathbf{v}_2) + C\mathbf{v}_3 + D\mathbf{v}_4 = 0 . \quad (\text{S39})$$

We break the coefficients into real and imaginary parts:  $A = A' + iA''$ ,  $B = B' + iB''$ ,  $C = C' + iC''$ ,  $D = D' + iD''$ . The equation becomes two equations, one for the real and one for the imaginary parts:

$$(A' + B')\mathbf{v}_1 + (-A'' + B'')\mathbf{v}_2 + C'\mathbf{v}_3 + D'\mathbf{v}_4 = 0 , \quad (\text{S40})$$

$$(A'' + B'')\mathbf{v}_1 + (A' - B')\mathbf{v}_2 + C''\mathbf{v}_3 + D''\mathbf{v}_4 = 0 . \quad (\text{S41})$$

With the correct choice of overall phase, we can guarantee one coefficient is real. We choose  $D$ , i.e.,  $D'' = 0$ . The imaginary equation then becomes

$$(A'' + B'')\mathbf{v}_1 + (A' - B')\mathbf{v}_2 + C''\mathbf{v}_3 = 0 . \quad (\text{S42})$$

The imaginary equation is now overdetermined. Since  $\mathbf{v}_1$ ,  $\mathbf{v}_2$ , and  $\mathbf{v}_3$  are in general linearly independent,  $A'' + B'' = 0$  and  $A' - B' = 0$ , i.e.,  $A = B^*$ , and furthermore  $C'' = 0$ , i.e.,  $C$  is real. Therefore there are still only four degrees of freedom. Furthermore, since  $C$  and  $D$  are both real and their eigenfunctions are both real, the  $0\pm$  branch of the wavefunction is real. It is apparent from Eq. (21) that both  $1\pm$  eigenfunctions belong to the  $1-$  branch, and these eigenfunctions are complex conjugates for any  $\rho$ , so the  $1\pm$  branch of the wavefunction is real. Therefore the wavefunction  $\langle \rho, \phi = 0 | \psi_{F_z} \rangle$  is real, despite the complex  $K_{1\pm}$ .

### Case 2

If both  $\mathbf{v}_3$  and  $\mathbf{v}_4$  are imaginary, the same procedure applies, except we choose  $D$  to be imaginary. Now the real part is overdetermined, leading to the conclusion that  $A = -B^*$

and  $C$  is imaginary. The wavefunctions are still real.

### Case 3

Finally, consider the case in which of  $\mathbf{v}_3$ ,  $\mathbf{v}_4$  is real and the other is imaginary. Without loss of generality,  $\mathbf{v}_3$  is imaginary. We again choose the overall phase so  $D$  is real. Redefining  $\mathbf{v}_5 = -i\mathbf{v}_3$ , the real and imaginary equations become

$$(A' + B')\mathbf{v}_1 + (-A'' + B'')\mathbf{v}_2 - C''\mathbf{v}_5 + D'\mathbf{v}_4 = 0, \quad (\text{S43})$$

$$(A'' + B'')\mathbf{v}_1 + (A' - B')\mathbf{v}_2 + C'\mathbf{v}_5 = 0. \quad (\text{S44})$$

The imaginary equation is overdetermined, in general  $\mathbf{v}_1$ ,  $\mathbf{v}_2$ , and  $\mathbf{v}_5$  are linearly independent, so again  $(A'' + B'') = 0$  and  $(A' - B') = 0$ , i.e.,  $A = B^*$ , and now  $C' = 0$ , so  $C$  is pure imaginary. By similar logic, there are 4 degrees of freedom and the wavefunctions are real.

## V. OSCILLATOR TRANSITION STRENGTH

The relative oscillator transition strength is determined by the square of the inner product of the light polarization vector,  $\hat{\mathbf{e}}$ , and the transition matrix element  $\mathcal{P} = \langle \Psi_{F_z} | \hat{\mathbf{p}} | \mathcal{G} \rangle$  between the vacuum state of the QD  $|\mathcal{G}\rangle$  and the exciton wavefunction  $|\Psi_{F_z}\rangle$  where  $\hat{\mathbf{p}}$  is the momentum operator. In the weak confinement regime where the exciton radius is much smaller than QD size the exciton wavefunction can be presented as  $\Psi_{F_z;n,m}(\mathbf{r}, \boldsymbol{\rho}) = \phi_{n,m}(\mathbf{r})|\psi\rangle_{F_z}(\rho, \phi)$ , [3, 4] where  $\phi_{n,m}(\mathbf{r})$  describes the internal motion of an electron and a hole within the 2D exciton and  $|\psi\rangle_{F_z}(\rho, \phi)$  from Eq. (22) describes the exciton center-of-mass motion in the cylindrical QDs. We consider the total exciton wavefunction from Eq. (14):

$$\Psi_{F_z}(\mathbf{r}, \rho, \phi, z) = \frac{2}{\mathcal{L}} \cos\left(\frac{\pi z_e}{\mathcal{L}}\right) \cos\left(\frac{\pi z_h}{\mathcal{L}}\right) \phi_{m,n}(\mathbf{r}) \times \frac{\mathcal{N}}{\sqrt{2\pi}} \left[ e^{iF_z\phi} \mathcal{R}_{0,0}^{F_z}(\rho) |0, 0\rangle + \sum_{\mu=\pm 1,0} e^{i(F_z-\mu)\phi} \mathcal{R}_{1,\mu}^{F_z}(\rho) |1, \mu\rangle \right].$$

The wavefunction describing the relative motion of the electron and hole is normalized. As a result the constant  $\mathcal{N}$  is connected only with exciton center-of-mass motion, and is defined

as:

$$\begin{aligned}
1 &= \mathcal{N}^2 \int_0^R \rho d\rho \left( |\mathcal{R}_{0,0}^{F_z}(\rho)|^2 + \sum_{\mu=\pm 1,0} |\mathcal{R}_{1,\mu}^{F_z}(\rho)|^2 \right) \\
&= \mathcal{N}^2 R^2 \int_0^1 x dx \left( |\mathcal{R}_{0,0}^{F_z}(Rx)|^2 + \sum_{\mu=\pm 1,0} |\mathcal{R}_{1,\mu}^{F_z}(Rx)|^2 \right). \tag{S45}
\end{aligned}$$

From the normalization condition, we have

$$\mathcal{N} = \frac{1}{R\sqrt{\mathcal{I}}}, \quad \mathcal{I} = \int_0^1 x dx \left( |\mathcal{R}_{0,0}^{F_z}(Rx)|^2 + \sum_{\mu=\pm 1,0} |\mathcal{R}_{1,\mu}^{F_z}(Rx)|^2 \right), \tag{S46}$$

where  $\mathcal{I}$  is a dimensionless normalization integral. Then, using the coordinate representation for the vacuum function,  $\mathcal{G} = \delta(\rho_e - \rho_h)$ , we calculate the transition dipole  $\mathbf{P}_{F_z}$  as,

$$\begin{aligned}
\mathbf{P}_{F_z;n,m}^\dagger &= \langle \mathcal{G} | \hat{\mathbf{p}} | \Psi_{F_z;n,m} \rangle \\
&= \frac{\mathcal{N}}{\sqrt{2\pi}} \phi_{n,m}(0) \sum_\nu \int_0^{2\pi} d\phi \int_0^R d^2\rho e^{i(F_z-\nu)\phi} \mathcal{R}_{1,\nu}^{F_z}(\rho) \langle \mathcal{G} | \hat{\mathbf{p}} | 1, \nu \rangle \\
&= \sqrt{2\pi} \mathcal{N} \phi_{n,m}(0) \int_0^R \rho d\rho \mathcal{R}_{1,\nu}^{F_z}(\rho) \langle \mathcal{G} | \hat{\mathbf{p}} | 1, \nu \rangle \delta_{F_z-\nu,0} \\
&= \sqrt{2\pi} \mathcal{N} \phi_{n,m}(0) R^2 \int_0^1 x dx \mathcal{R}_{1,\nu}^{F_z}(Rx) \langle \mathcal{G} | \hat{\mathbf{p}} | 1, \nu \rangle \delta_{F_z-\nu,0}. \tag{S47}
\end{aligned}$$

Then the square of the dipole matrix element is,

$$|\langle \mathcal{G} | \hat{\mathbf{p}} | \Psi_{F_z;n,m} \rangle|^2 = \frac{2\pi R^2}{\mathcal{I}} |\phi_{n,m}(0)|^2 \left| \int_0^1 x dx \mathcal{R}_{1,\nu}^{F_z}(Rx) \right|^2 |\langle \mathcal{G} | \hat{\mathbf{p}} | 1, \nu \rangle|^2 \delta_{F_z-\nu,0}. \tag{S48}$$

It is most useful to recast this in terms of the oscillator strength per unit area for light with polarization vectors denoted  $\hat{e}$ , using  $f_{\hat{e}}^{F_z;n,m} = 2|\mathbf{P}_{F_z;n,m} \cdot \hat{e}|^2 / (m_0 \hbar \omega)$ , where  $\hbar \omega$  is the transition energy and  $P_{F_z;n,m}$  is the dipole transition matrix element for exciton state  $F_z$ :

$$\frac{f_{\hat{e}}^{F_z}}{\pi R^2} = \left( \frac{\mathcal{K}_{F_z,\nu}^2}{\pi R^2} \right) \frac{2|\langle \mathcal{G} | \hat{\mathbf{p}} | 1, \nu \rangle \cdot \hat{e}|^2}{m_0 \hbar \omega} \delta_{F_z-\nu,0}, \tag{S49}$$

where the squared overlap per unit area is,

$$\left( \frac{\mathcal{K}_{F_z,\nu}^2}{\pi R^2} \right) = \frac{2}{\mathcal{I}} |\phi_{n,m}(0)|^2 \left| \int_0^1 x dx \mathcal{R}_{1,\nu}^{F_z}(Rx) \right|^2 \delta_{F_z-\nu,0}. \tag{S50}$$

As a dimensional check we note that  $\mathcal{I}$  is the dimensionless normalization integral while the overlap integral on the right side is also dimensionless. Using the variationally determined internal wavefunction,

$$\phi_{1,0}(\mathbf{r}_e - \mathbf{r}_h; a_{1,0}) = \frac{4}{a_{1,0}} \frac{1}{\sqrt{2\pi}} e^{-2|r|/a_{1,0}} , \quad |\phi_{n,m}(0)|^2 = \frac{8}{\pi a_{1,0}^2} . \quad (\text{S51})$$

From this we see that the right-hand side of Eq. (S50) has dimensions of inverse area.

Next we examine the dipole matrix elements  $\langle \mathcal{G} | \hat{\mathbf{p}} | 1, \nu \rangle$ . Using the crystal field model for the Bloch functions in 2D MHPs presented in Ref. 5–8 which was applied to determine the dipole matrix elements in Refs. 1–3 we find,

$$\begin{aligned} \langle 1, 0 | \hat{\mathbf{p}} | \mathcal{G} \rangle &= g_0 P_{\text{cv}} \hat{z} , & \langle 1, \pm 1 | \hat{\mathbf{p}} | \mathcal{G} \rangle &= g_{\pm 1} P_{\text{cv}} \frac{(\mp \hat{x} + i \hat{y})}{\sqrt{2}} , \\ g_0 &= \sqrt{2} \sin \theta , & g_{\pm 1} &= \cos \theta , \end{aligned} \quad (\text{S52})$$

where  $P_{\text{cv}} = -i \langle S | \hat{\mathbf{p}}_z | Z \rangle$  is the Kane momentum matrix element, and  $\theta$  is the crystal field phase angle from Eq. (9), which is given by [1]

$$\tan 2\theta = \frac{2\sqrt{2}\Delta_{\text{SO}}}{\Delta_{\text{SO}} - 3\delta} \quad \theta \leq \frac{\pi}{2} , \quad (\text{S53})$$

where  $\Delta_{\text{SO}}$  is the spin-orbit splitting and  $\delta$  is the tetragonal crystal field parameter. As shown in Table 1, we use an experimental value of  $\sin \theta = 0.227$  [7] in our numerical calculations.

As a check of the polarization properties of Eq. (S52), we note that for absorption, from ground state  $|\mathcal{G}\rangle$  to exciton state  $|\Psi_{F_z}\rangle$ , we need the matrix elements  $\langle \Psi_{F_z} | \hat{\mathbf{p}} | \mathcal{G} \rangle \cdot \hat{e}$ . We see from above Eq. (S52) that a state  $|1, \pm 1\rangle$  will absorb light with polarization  $\hat{e} = (\hat{x} \pm i \hat{y})/\sqrt{2}$ , corresponding to angular momentum  $\pm 1$  as required by conservation of angular momentum.

Now, using the expressions Eq. (S52) we can finally write an expression for the oscillator strength per unit area of the states in a quantum disk. We will use the definition of the Kane energy,

$$E_p \equiv \frac{2|P_{\text{cv}}|^2}{m_0} . \quad (\text{S54})$$

The Kane energy may be estimated from experiment, as discussed in the main text.

We consider light with polarization vectors denoted  $\hat{\mathbf{e}}_\mu$  given as,

$$\hat{\mathbf{e}}_0 = \hat{\mathbf{z}} , \quad (\text{S55})$$

$$\hat{\mathbf{e}}_{\pm 1} = \frac{\hat{\mathbf{x}} \pm i \hat{\mathbf{y}}}{\sqrt{2}} . \quad (\text{S56})$$

We define  $f_{\mu}^{F_z}$  to be the oscillator strength for this polarization, that is,  $f_{\pm 1}$  denotes the oscillator strength for circular polarized light propagating with wave vector along the  $+\hat{z}$  direction, with positive (+) and negative (-) helicity, while  $f_0$  denotes linearly polarized light with polarization vector along  $\hat{z}$ . Then we have,

$$f_0^{F_z} = 2 \sin^2(\theta) \mathcal{K}_{F_z,0}^2 \left( \frac{E_p}{\hbar\omega} \right) \delta_{F_z,0} , \quad f_{\pm 1}^{F_z} = \cos^2(\theta) \mathcal{K}_{F_z,\pm 1}^2 \left( \frac{E_p}{\hbar\omega} \right) \delta_{F_z,\pm 1} . \quad (\text{S57})$$

Note again, the phase angle  $\theta$  reflects the crystal field; since  $\sin \theta$  is small, the oscillator strength  $f_0 \ll f_{\pm 1}$ .

## VI. LONG-RANGE EXCHANGE

In order to calculate the long-range exchange, we need to calculate the polarization and then evaluate the integral over the quantum disk in Eq. (29). The exciton total wavefunction was given in Eq. (14):

$$\Psi_{F_z}(\mathbf{r}, \rho, \phi, z) = \frac{2}{\mathcal{L}} \cos\left(\frac{\pi z_e}{\mathcal{L}}\right) \cos\left(\frac{\pi z_h}{\mathcal{L}}\right) \phi_{m,n}(\mathbf{r}) \times \frac{\mathcal{N}}{\sqrt{2\pi}} \left[ e^{iF_z\phi} \mathcal{R}_{0,0}^{F_z}(\rho) |0,0\rangle + \sum_{\mu=\pm 1,0} e^{i(F_z-\mu)\phi} \mathcal{R}_{1,\mu}^{F_z}(\rho) |1,\mu\rangle \right] .$$

The polarization is

$$\mathcal{P}_{F_z}^\dagger = i \frac{\hbar e}{m_0 \hbar \omega} \frac{2}{\mathcal{L}} \cos^2\left(\frac{\pi z}{\mathcal{L}}\right) \phi_{n,m}(0) \frac{\mathcal{N}}{\sqrt{2\pi}} \sum_{\nu} e^{i(F_z-\nu)\phi} \mathcal{R}_{1,\nu}^{F_z}(\rho) \langle \mathcal{G} | \hat{\mathbf{p}} | 1, \nu \rangle . \quad (\text{S58})$$

Using this expression in Eq. (29) we can now calculate the LR exchange corrections. Referring to Eq. (S52) we recast the dipole matrix element as,

$$\langle \mathcal{G} | \hat{\mathbf{p}} | 1, \nu \rangle = P_{cv} g_{\nu} \hat{\mathbf{e}}_{\nu} . \quad (\text{S59})$$

Then, the polarization takes the form,

$$\begin{aligned} \mathcal{P}_{F_z}^\dagger &= i \frac{P_{cv} \hbar e}{m_0 \hbar \omega} \frac{2}{\mathcal{L}} \cos^2\left(\frac{\pi z}{\mathcal{L}}\right) \phi_{n,m}(0) \frac{\mathcal{N}}{\sqrt{2\pi}} \sum_{\nu} e^{i(F_z-\nu)\phi} \mathcal{R}_{1,\nu}^{F_z}(\rho) g_{\nu} \hat{\mathbf{e}}_{\nu} , \\ &\equiv i \frac{P_{cv} \hbar e}{m_0 \hbar \omega} \sum_{\nu} \mathcal{F}_{F_z,\nu}(\rho, \phi, z) \hat{\mathbf{e}}_{\nu} , \end{aligned} \quad (\text{S60})$$

where we have defined the functions  $\mathcal{F}_{F_z,\nu}(\rho, \phi, z)$  as,

$$\mathcal{F}_{F_z,\nu}(\rho, \phi, z) \equiv \frac{2}{\mathcal{L}} \cos^2\left(\frac{\pi z}{\mathcal{L}}\right) \phi_{n,m}(0) \frac{\mathcal{N}}{\sqrt{2\pi}} e^{i(F_z-\nu)\phi} \mathcal{R}_{1,\nu}^{F_z}(\rho) g_{\nu} , \quad (\text{S61})$$

where  $\mathcal{N}$  is the normalization integral defined in Eq. (S46).

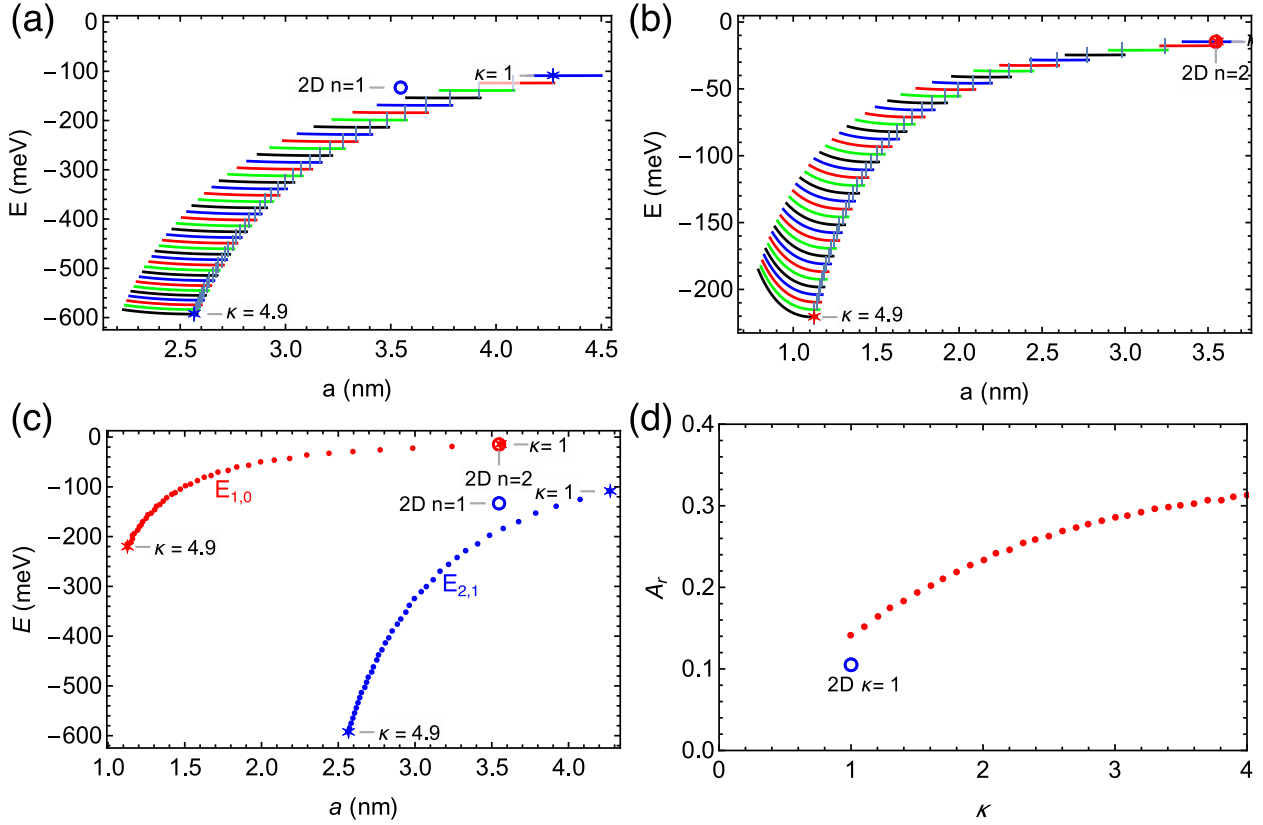


Figure S-1. Results of the variational calculation of the ground state and first excited state of the internal motion. In each panel, the value calculated in the 2D limit is shown as an open circle. (a) Energy versus  $a$  using the ground-state hydrogenic ansatz  $\phi_{1,0}(\rho; a) \sim \exp(-2\rho/a)$ . Dielectric constant ratio  $\kappa = \epsilon_i/\epsilon_o$  varies in steps of 0.1 from  $\kappa = 1$  to  $\kappa = 4.9$ . The optimum value is indicated for each  $\kappa$  on the curve. Using the values from Table 1,  $\kappa = 3.2$ . (b) Energy versus  $a$  using the excited-state hydrogenic ansatz  $\phi_{2,\pm 1}(r, \phi; a_{2,1}) \sim \rho \exp(-2\rho/3a_{2,1}) \exp(\pm i\phi)$ . (c) Optimized ground-state binding energy  $E_{1,0}$  and excited-state energy  $E_{2,1}$ . (d) Geometric Rashba factor  $A_R^C$  given by Eq. (6). The calculated value for the parameters in Table 1 is shown in Supplementary Table S-1.

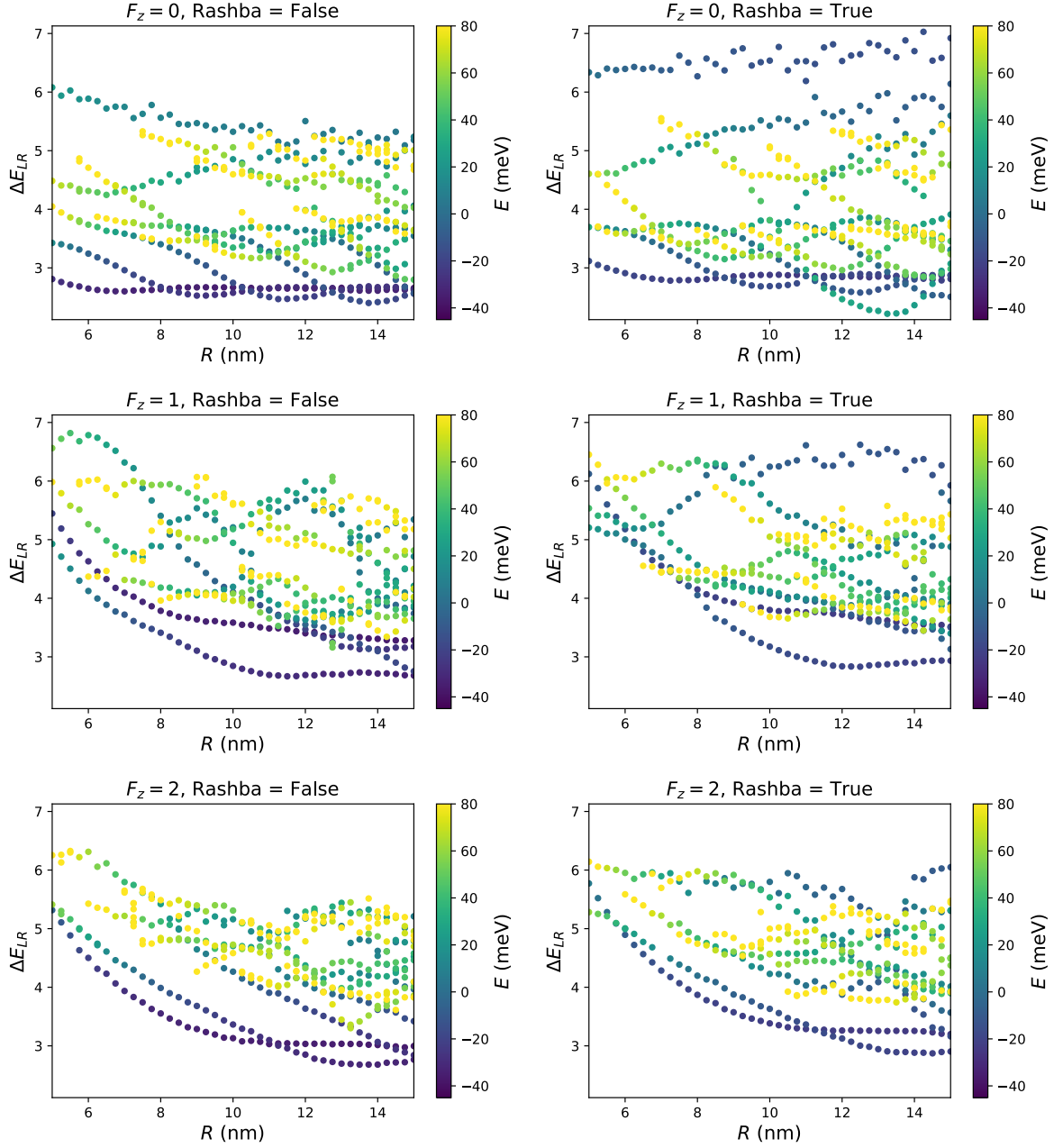


Figure S-2. Long-range exchange correction included in the states shown in Figure 3. The color indicates the energy of the state in the absence of long-range exchange correction. The relatively small size and spread of the LR exchange gives us confidence in treating LR exchange perturbatively.

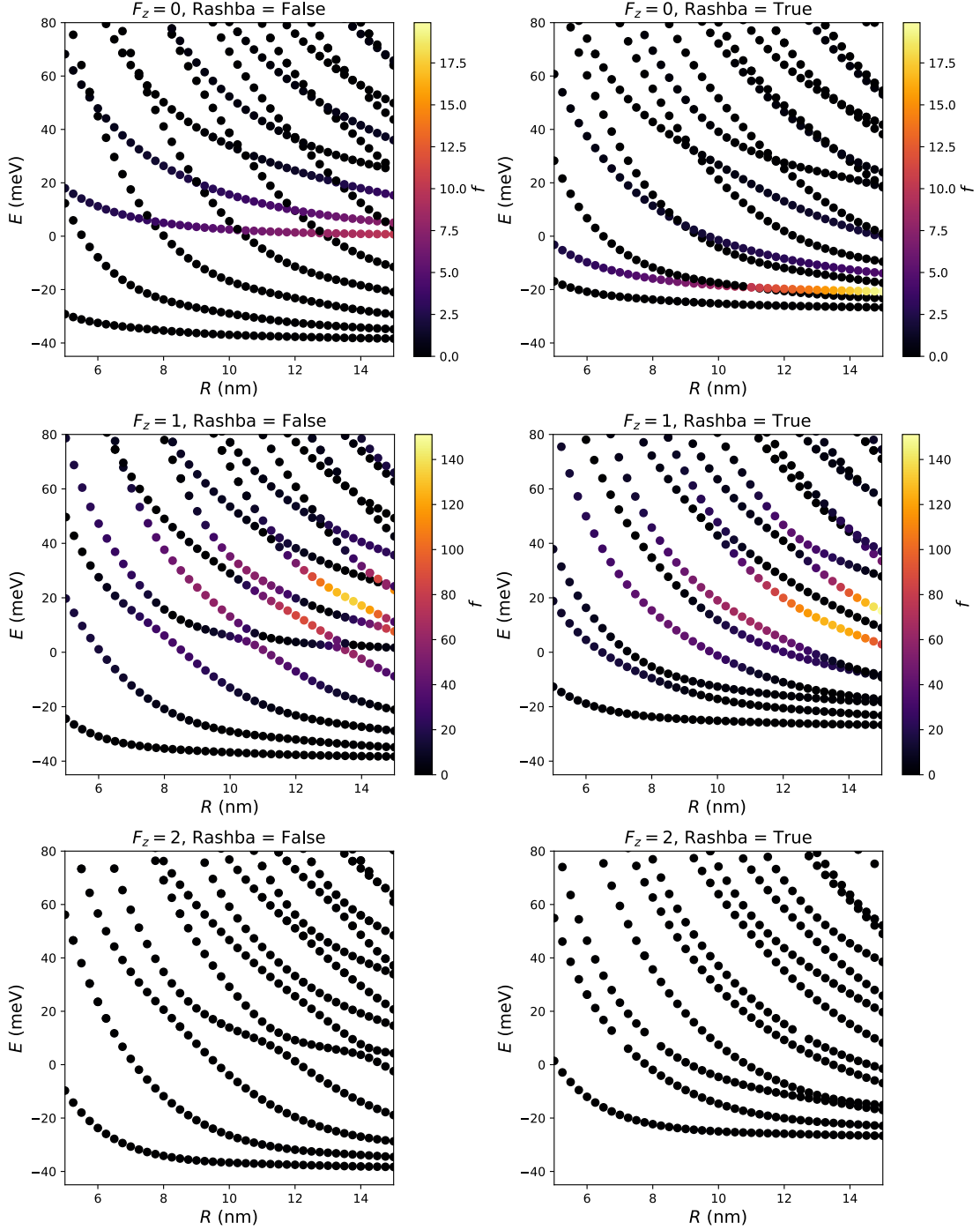


Figure S-3. Energy levels of confined wavefunctions as a function of disk radius  $R$  (as in Figure 3) but without the LR exchange corrections. Rows are  $F_z = 0$  (top),  $F_z = 1$  (middle), and  $F_z = 2$  (bottom), and columns are without and with internal Rashba from the left. The total oscillator strength  $f$  of the states as given by Eq. (25) is indicated by the color of the points. The results are qualitatively very similar to Figure 3. The avoided crossings can be seen more easily in this version, since the LR contribution is not included self-consistently in the wavefunctions.

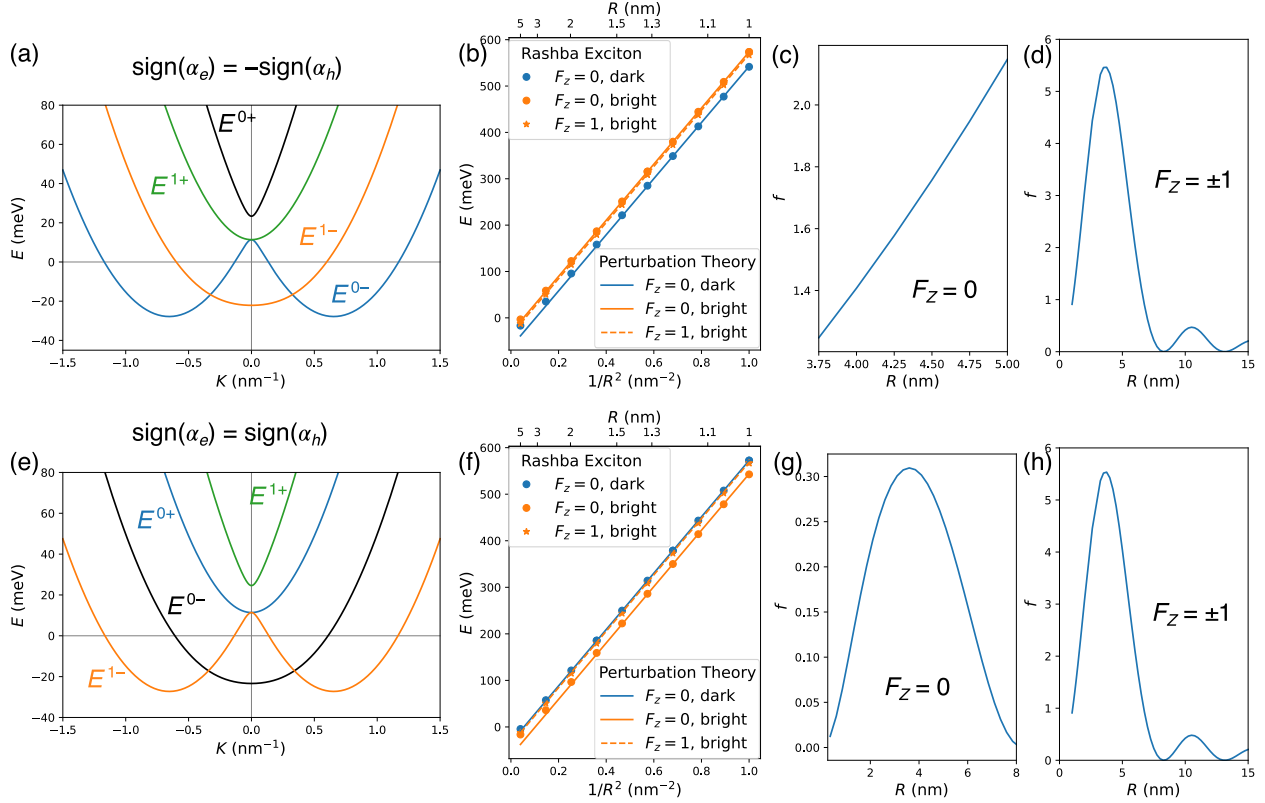


Figure S-4. Comparison of same-sign and opposite-sign cases for small QDs. Panels (a-d) use the opposite sign for  $\alpha_e$  and  $\alpha_h$  (as is assumed elsewhere in the paper) while panels (e-h) use the same sign. (a) and (e) show the dispersion. (b) and (f) show the energy levels (neglecting LR exchange) for small QDs as a function of  $1/R^2$ . As expected, we see four parallel lines (dark and bright  $F_z = 0$ , two degenerate  $F_z = \pm 1$ ) with the dark and bright  $F_z = 0$  states switching position between the cases. The energies approach the results from perturbation theory, which are shown by lines and described by  $E^{F_z}(R) = \frac{\hbar^2(2.405)^2}{2MR^2} - 2A_r^{\text{COM}}(E_r^e + E_r^h) + E_{\text{exch}}^{F_z}$ , where the first term represents COM confinement, the second term is an overall shift due to COM Rashba terms in Eq. 2, and the exchange terms  $E_{\text{exch}}^{F_z}$  represent the sum of SR exchange and Rashba internal motion terms. The exchange terms are given by  $E_{\text{exch}}^{F_z=1} = w \cos^2 \theta$ ,  $E_{\text{exch}}^{F_z=0, \text{bright}} = 2w \sin^2 \theta - 4(A_r^{\text{COM}} - A_r^{\text{REL}})\mathcal{E}_R$ , and  $E_{\text{exch}}^{F_z=0, \text{dark}} = 4(A_r^{\text{COM}} - A_r^{\text{REL}})\mathcal{E}_R$ .  $A_r^{\text{COM}} \approx 0.48$  is the COM Rashba coefficient [9] and  $A_r^{\text{REL}} \approx 0.292$  is the relative Rashba coefficient. Oscillator strengths (OS) are shown as a function of  $R$  in panels (c, d, g, h). In the opposite-sign case, OS of the  $F_z = 0$  bright state (c) is monotonically increasing with  $R$ , whereas in the same-sign case, it peaks at intermediate  $R$  and goes to zero in both the  $R \rightarrow 0$  limit (as expected from the perturbative treatment [9]) and the  $R \rightarrow \infty$  limit (due to the indirect nature of the bulk dispersion). The oscillator strengths of the lowest  $F_z = \pm 1$  state are similar in both cases (d) and (h).

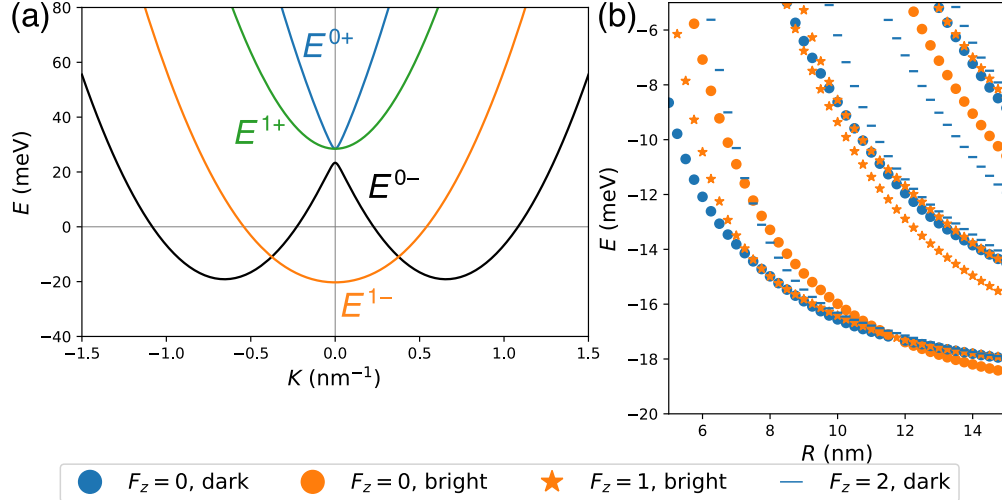


Figure S-5. Illustration that the model can produce a bright ground exciton. These plots use the same parameters as in the rest of the paper, but with an increased short-range exchange constant  $w = 30$  meV, a value representative of  $\text{PbBr}_4$ -based 2D HOIPs, [8]. Internal Rashba is included, LR exchange corrections are not included. (a) bulk exciton dispersion. The bright state at  $K = 0$  from the  $E^{1-}$  branch is the energy minimum, and the  $E^{0-}$  state is dark at  $K = 0$ . (b) Low-energy levels as a function of QD radius  $R$ . Color indicates whether the state is bright (optically active, shown in orange) or dark (optically passive, shown in blue) and shape indicates  $F_z$  as in Figure 4 (circles for  $F_z = 0$ , stars for  $F_z = 1$ , and lines for  $F_z = 2$ ). For  $R \gtrsim 12$  nm, the ground state is a bright  $F_z = 0$  state.

- 
- [1] P. C. Sercel, J. L. Lyons, D. Wickramaratne, R. Vaxenburg, N. Bernstein, and Al. L. Efros, Exciton fine structure in perovskite nanocrystals, *Nano Lett.* **19**, 4068 (2019).
- [2] P. C. Sercel, J. L. Lyons, N. Bernstein, and Al. L. Efros, Quasicubic model for metal halide perovskites, *J. Chem. Phys.* **151**, 234106 (2019).
- [3] M. Gramlich, M. W. Swift, J. L. Lyons, Al. L. Efros, P. C. Sercel, and A. Urban, Dark and bright excitons in halide perovskite nanoplatelets (2021), (submitted).
- [4] Al. L. Efros and A. L. Efros, Interband absorption of light in a semiconductor sphere, *Sov. Phys. Semicond.* **16**, 772 (1982).

- [5] Y. Nagamune, S. Takeyama, and N. Miura, Exciton spectra and anisotropic Zeeman effect in  $\text{PbI}_2$  at high magnetic fields up to 40 T, *Phys. Rev. B* **43**, 12401 (1991).
- [6] K. Tanaka, K. T. Takahashi, T., K. Umeda, K. Ema, T. Umebayashi, K. Asai, K. Uchida, and N. Miura, Electronic and excitonic structures of inorganic-organic perovskite-type quantum-well crystal  $(\text{C}_4\text{H}_9\text{NH}_3)_2\text{PbBr}_4$ , *Jpn. J. Appl. Phys., Part 2* **44**, 5923 (2005).
- [7] T. Kataoka, T. Kondo, R. Ito, S. Kazuhito, K. Uchida, and N. Miura, Magneto-optical study on excitonic spectra in  $(\text{C}_6\text{H}_{13}\text{NH}_3)_2\text{PbI}_4$ , *Phys. Rev. B* **47**, 2010 (1993).
- [8] K. Ema, K. Umeda, M. Toda, C. Yajima, Y. Arai, and H. Kunugita, Huge exchange energy and fine structure of excitons in an organic-inorganic quantum well material, *Phys. Rev. B* **73**, 241310(R) (2006).
- [9] M. A. Becker, R. Vaxenburg, G. Nedelcu, P. C. Sercel, A. Shabaev, M. J. Mehl, J. G. Michopoulos, S. G. Lambrakos, N. Bernstein, J. L. Lyons, T. Stöferle, R. F. Mahrt, M. V. Kovalenko, D. J. Norris, G. Raino, and Al. L. Efros, Bright triplet excitons in caesium lead halide perovskites, *Nature* **553**, 189 (2018).